Distinct molecular pathways govern presynaptic homeostatic plasticity

Anu G. Nair[1,2], Paola Muttathukunnel[1,3], Martin Müller[1,3,*]

[1]Department of Molecular Life Sciences, University of Zurich, Winterthurerstrasse 190, 8057 Zurich, Switzerland

[2]Department of Neuroscience, Karolinska Institutet, 17177 Stockholm, Sweden

[3]Neuroscience Center Zurich, University of Zurich/ETH Zurich, 8057 Zurich, Switzerland

* martin.mueller@mls.uzh.ch

Abstract

Presynaptic homeostatic plasticity (PHP) stabilizes synaptic transmission by counteracting impaired neurotransmitter receptor function through increased presynaptic release. PHP is thought to be triggered by impaired receptor function, and to involve a stereotypic signaling pathway. However, here we demonstrate that different receptor perturbations that similarly impair synaptic activity result in vastly different responses at the *Drosophila* neuromuscular junction. While competitive receptor inhibition is not compensated by PHP, receptor pore block and allosteric inhibition induce compensatory PHP. Intriguingly, PHP triggered by receptor pore block and allosteric inhibition involve distinct presynaptic adaptations, including differential modulation of the active-zone scaffold Bruchpilot and short-term plasticity. Moreover, while PHP upon allosteric receptor inhibition does not require molecules underlying pore-block induced PHP (RIM and dysbindin), it is promoted by presynaptic Protein Kinase D. Thus, synapses not only respond differentially to similar activity impairments, but achieve homeostatic compensation via distinct mechanisms, highlighting the diversity of homeostatic signaling.

Introduction

A variety of homeostatic signaling systems stabilize neural function by counteracting diverse perturbations (Delvendahl et al., 2019; Frank et al., 2006; Ibata et al., 2008; Keck et al., 2013; Petersen et al., 1997; Teichert et al., 2017; Turrigiano et al., 1998). Chemical synapses compensate for neural activity perturbations through homeostatic regulation of neurotransmitter release (Frank et al., 2006; Petersen et al., 1997) or neurotransmitter receptors (Turrigiano et al., 1998). There are also emerging links between homeostatic synaptic plasticity and neural disease, such as autism spectrum disorders, schizophrenia, or amyotrophic lateral sclerosis (Genç et al., 2020; Perry et al., 2017; Tatavarty et al., 2020).

Presynaptic homeostatic plasticity (PHP) is a major form of homeostatic plasticity that is characterized by homeostatic upregulation of presynaptic release in response to reduced postsynaptic neurotransmitter receptor function (Delvendahl and Müller, 2019). PHP has been observed at diverse synapses in different species (Delvendahl et al., 2019; Frank et al., 2006; Wang et al., 2018), implying evolutionary conservation. PHP is mostly induced by pharmacological or genetic neurotransmitter receptor impairment (Frank et al., 2006; Petersen et al., 1997). Correspondingly, impaired receptor function is thought to trigger homeostatic signaling. In this regard, Ca^{2+} flux through postsynaptic receptors has been hypothesized to be a major synaptic variable sensed by the signaling system promoting PHP (Frank et al., 2006; Ouanounou et al., 2016; Wang et al., 2016). In agreement, postsynaptic signaling by CaMKII and the Ca^{2+}-binding protein Peflin has been implicated in PHP at the *Drosophila* neuromuscular junction (NMJ) (Kikuma et al., 2019; Li et al., 2018). However, PHP can be induced in the absence of extracellular Ca^{2+} at the *Drosophila* NMJ (Goel et al., 2017). Moreover, there is some evidence that ion flux through nicotinic acetylcholine receptors is dispensable for PHP at the mouse NMJ (Wang et al., 2018). It is thus currently unclear whether PHP is triggered by impaired synaptic function resulting from receptor inhibition.

The molecular mechanisms underlying PHP are understood best at the *Drosophila* NMJ. At this synapse, PHP can be rapidly expressed within minutes after pharmacological receptor perturbation by the glutamate receptor (GluR) pore blocker Philanthotoxin-433 (PhTx) (Frank et al., 2006). Moreover, PHP can be chronically sustained upon genetic receptor impairment imposed by loss of the GluRIIA subunit (Petersen et al., 1997). Electrophysiology-based genetic screens at the *Drosophila* NMJ have discovered several genes that are required for PHP, including the schizophrenia-susceptibility gene *dysbindin* (Dickman and Davis, 2009), or the gene encoding the active zone protein rab3-interacting molecule (RIM) (Müller et al., 2012). Most of the identified genes are required for both, rapid and chronic PHP expression upon pharmacological or genetic receptor impairment, implying that a stereotypic signaling system promotes acute and chronic PHP. However, recent work revealed that some genes that are required for chronic PHP are dispensable for acute PHP (Böhme et al., 2019; James et al., 2019). These findings either suggest that different molecular mechanisms underlie different PHP phases – early induction vs. chronic maintenance. Alternatively, different modes of receptor perturbation – receptor pore block vs. subunit loss – could trigger distinct molecular pathways, independent of the PHP phase. However, whether different modes of receptor perturbation promote PHP via distinct molecular mechanisms remains untested.

Here, we tested this idea by investigating the effects of different acute receptor perturbations on PHP at the *Drosophila* NMJ. Despite a similar degree of synaptic activity impairment, PHP was induced by glutamate receptor pore block and allosteric inhibition, but not by competitive antagonism. Moreover, PHP induced by pore block (PhTx) and allosteric inhibition (Gyki) exhibited marked differences in the regulation of short-term plasticity and active-zone structure. Importantly, PHP induced by PhTx and Gyki involved distinct underlying signaling molecules. Whereas PhTx-induced PHP relied on the known PHP genes *dysbindin* and *RIM*, Gyki-induced PHP is promoted by presynaptic Protein Kinase D (PKD). Together, our data suggest that impaired receptor function *per se* is not sufficient to induce PHP. Instead,

PHP could be induced by distinct homeostatic pathways depending on the specific way postsynaptic receptors are perturbed.

Results

PHP depends on the type of GluR perturbation

To examine whether distinct receptor perturbations could induce PHP via different underlying signaling, we investigated the acute form of PHP at the *Drosophila* larval NMJ after glutamate receptor (GluR) perturbation using three different antagonists: PhTx, γ-D-Glutamylglycine (γDGG) and Gyki-53655 (Gyki) (Fig. 1A). These antagonists inhibit GluRs through different modes: While PhTx is an activity-dependent pore blocker (Piek, 1982), γDGG acts as a low-affinity competitive antagonist (Liu et al., 1999), and Gyki is an allosteric inhibitor (Balannik et al., 2005) (Fig. 1A).

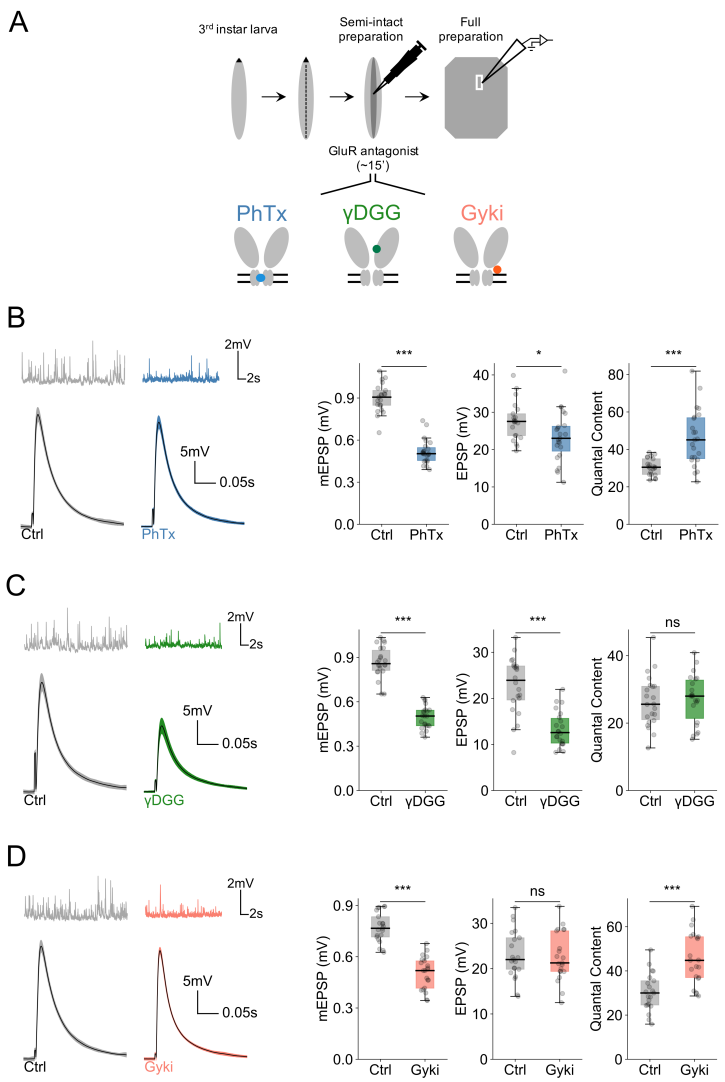

*Fig 1. Distinct glutamate receptor perturbations produce different presynaptic homeostatic plasticity (PHP) responses. (**A**) Scheme of NMJ treatment with different receptor inhibitors. Dorsally dissected, "semi-intact" 3rd instar Drosophila larvae were incubated with one of the three listed inhibitors (PhTx (20 μM) - receptor pore blocker; γDGG (5 mM) - competitive antagonist; Gyki (10 μM) - allosteric antagonist) for 15 minutes, followed by full dissection and electrophysiology. (**B**) Representative traces (mEPSPs and EPSPs), mEPSP amplitudes, EPSP amplitudes and quantal content of saline (Ctrl) or PhTx-treated NMJs. PhTx treatment increased quantal content, indicating PHP. n = 21 (Ctrl) vs 23 (PhTx). $[Ca^{2+}]_e$ = 0.3 mM. (**C**) Representative traces (mEPSPs and EPSPs), mEPSP amplitudes, EPSP amplitudes and quantal content of saline (Ctrl) or γDGG-treated NMJs. γDGG did not affect quantal content, indicating no PHP expression. n = 22 (Ctrl) vs 22 (γDGG). $[Ca^{2+}]_e$ = 0.3 mM. (**D**) Representative traces (mEPSPs and EPSPs), mEPSP amplitudes, EPSP amplitudes and quantal content of saline (Ctrl) or Gyki-treated NMJs. Gyki treatment increased quantal content, indicating PHP. n = 21 (Ctrl) vs 21 (Gyki). $[Ca^{2+}]_e$ = 0.3 mM. Pairwise comparisons were done with a two-sided Mann Whitney U test. Each data point indicates the median value for a given cell. ns : p >= 0.05; * : p < 0.05; ** : p < 0.01; *** : p < 0.001.*

Application of PhTx at a sub-saturation concentration for ~15 minutes (Fig. 1A; see Material & Methods) robustly reduced the median mEPSP amplitude at the NMJ by ~50% compared to untreated controls (Fig. 1B), indicating robust postsynaptic receptor inhibition. By contrast, PhTx reduced the median AP-evoked EPSP amplitude by only

~15%, translating into a significant increase in quantal content (QC = EPSP/mEPSP) (Fig. 1B). The increase in quantal content upon PhTx treatment indicates a homeostatic increase in neurotransmitter release that restores EPSP amplitudes to baseline levels, consistent with PHP (Frank et al., 2006). Application of γDGG for ~15 minutes (see Material & Methods) reduced the median mEPSP amplitude by a similar magnitude as PhTx (Fig. 1C). In contrast to PhTx, the median EPSP amplitude also dropped proportional to the mEPSP amplitude reduction in the presence of γDGG (Fig. 1C). Consequently, there was no increase in quantal content (Fig. 1C), demonstrating that receptor inhibition by γDGG does not result in PHP. Finally, Gyki incubation for 15 minutes (see Material & Methods) significantly decreased mEPSP amplitudes, but EPSP amplitudes were comparable to untreated controls, translating into a significant increase in quantal content (Fig. 1D). This indicates rapid and robust PHP expression within 15 minutes upon Gyki treatment (Fig. 1B). Since PhTx, γDGG and Gyki reduced receptor function by a similar magnitude (Fig. 1C-D), but only PhTx and Gyki resulted in homeostatic compensation, these results indicate that a general reduction in GluR function is not sufficient to produce PHP, highlighting that the specific way receptors are perturbed is an important determinant of homeostatic signaling. As PhTx and Gyki interact differently with GluRs, this could also mean that there may be differences in the resulting PHP process.

Gyki induces PHP in the fully-dissected larval preparation

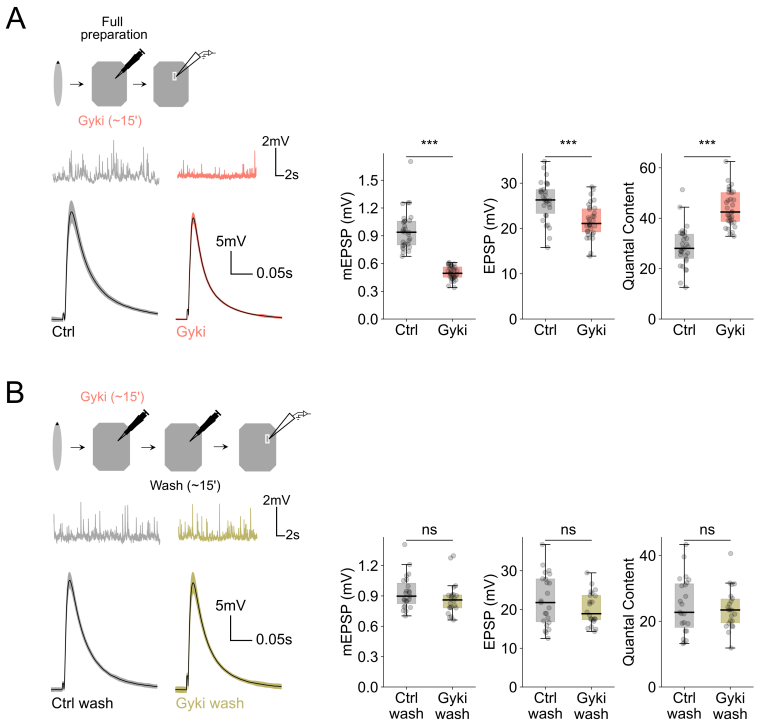

*Fig 2. Gyki reversibly induces PHP in the fully-dissected preparation. (**A**) Scheme of Gyki treatment on fully-dissected larval preparation along with representative traces (mEPSPs and EPSPs), median mEPSP amplitudes, median EPSP amplitudes and quantal content of saline (Ctrl) or Gyki-treated NMJs. Increased quantal content in the presence of Gyki indicated PHP. n = 30 (Ctrl) vs 32 (Gyki). $[Ca^{2+}]_e$ = 0.3 mM. (**B**) Scheme of Gyki reversibility experimental design with representative traces (mEPSPs and EPSPs), median mEPSP amplitudes, median EPSP amplitudes and quantal content of NMJs after saline (Ctrl) or Gyki washout. In these experiments, fully-dissected larval preparations were incubated with either saline (Ctrl wash) or Gyki (Gyki wash) for 15 minutes. This was followed by further incubation with saline for another 15 minutes. Similar mEPSP amplitudes between Ctrl and Gyki wash indicate full reversibility of Gyki-mediated receptor inhibition. Similar EPSP amplitudes and quantal content between the two groups indicate PHP reversibility after the 15-minute washout. n = 23 (Ctrl wash) vs 22 (Gyki wash). $[Ca^{2+}]_e$ = 0.3 mM. Pairwise comparisons were done with a two-sided Mann Whitney U test. Each data point indicates the median value for a given cell. ns : p >= 0.05; * : p < 0.05; ** : p < 0.01; *** : p < 0.001.*

Given that γDGG application does not result in any observable PHP, we focused the rest of our analysis on Gyki and PhTx. While PhTx has been used extensively to study PHP at the *Drosophila* NMJ, nothing is known about PHP in response to Gyki application. We therefore characterized PHP after Gyki treatment and compared it to PhTx-induced PHP.

PhTx only induces PHP when applied to “semi-intact”, i.e. not fully dissected, larval preparations (Frank et al., 2006). The reason for this is unknown, but it may be due to the involvement of some postsynaptic muscle compartment that is disrupted in a fully-dissected preparation (Frank et al., 2006).

We first tested whether Gyki could produce PHP when applied to the fully-dissected preparation (Fig. 2A). To this end, synaptic transmission was assayed after fully-dissected preparations were incubated with Gyki for 15 minutes (Fig. 2A; see Materials & Methods). Gyki resulted in a robust (~50%) reduction in the median mEPSP amplitude (Fig. 2A). By contrast, the reduction in the median AP-evoked EPSP amplitude was less pronounced than the decrease in mEPSP amplitude, resulting in a significant increase in quantal content (Fig. 2A). Thus, in contrast to PhTx (Frank et al., 2006), Gyki application rapidly induces PHP in the fully-dissected preparation, indicating possible differences between PHP induced by PhTx and Gyki.

Gyki reveals rapid PHP reversibility

Reversibility is a central feature of homeostatic systems in order to realize bi-directional regulation. PHP in response to pharmacological neurotransmitter receptor perturbation is reversible at the mammalian NMJ and in the mammalian CNS (Delvendahl et al., 2019; Wang et al., 2016). We next investigated PHP reversibility after GluR perturbation. At the *Drosophila* NMJ, GluR inhibition by PhTx is irreversible (Frank et al., 2006), precluding the use of PhTx to probe PHP reversibility. By contrast, mammalian AMPAR inhibition by Gyki is reversible (Balannik et al., 2005). Therefore, we tested whether Gyki reversibly blocks *Drosophila* GluRs. Fully-dissected preparations were either incubated with Gyki or saline for 15 minutes, followed by a wash and saline incubation for 15 minutes (Fig. 2B). mEPSP amplitudes recorded after this procedure were comparable between Gyki-treated and saline-treated NMJs (Fig. 2B), demonstrating that Gyki reversibly antagonizes *Drosophila* GluRs. Probing AP-evoked EPSPs 15 minutes after Gyki wash-out yielded similar EPSP amplitudes between the Gyki- and the control group (Fig. 2B). Correspondingly, quantal content between the two experimental groups showed no significant difference (Fig. 2B), indicating that PHP rapidly reverses within 15 minutes upon Gyki removal. Hence, in conjunction with its rapid induction within 15 minutes, PHP at the *Drosophila* NMJ is a highly dynamic process that reversibly controls synaptic efficacy on the minute time scale. These results also highlight the utility of Gyki as a receptor perturbation to explore mechanisms underlying PHP reversal at the *Drosophila* NMJ.

Gyki and PhTx increase RRP size with different effects on short-term plasticity

PhTx induces PHP by increasing readily releasable pool (RRP) size without any apparent effects on short-term plasticity during repetitive stimulation (Ortega et al., 2018; Weyhersmuller et al., 2011). To test RRP size modulation and short-term plasticity upon Gyki treatment, we performed two-electrode voltage clamp (TEVC) analysis at an elevated extracellular Ca^{2+} concentration ($[Ca^{2+}]_e$) near the physiological range (1.0 mM). First, we tested whether Gyki induces PHP at this $[Ca^{2+}]_e$. Gyki resulted in a pronounced reduction in the median mEPSP amplitude, similar to PhTx (Fig. 3A). By contrast, the reduction in AP-evoked EPSC amplitude was significantly less pronounced than the decrease in mEPSP amplitude, translating into a significant increase in apparent quantal content (EPSC/mEPSP; note that mEPSCs could not be recorded along with EPSCs, see Materials & Methods) (Fig. 3A). We conclude that Gyki also elicits PHP at near-physiological $[Ca^{2+}]_e$, similar to PhTx.

We next probed RRP size modulation during PHP induced by Gyki and compared it to PhTx using cumulative EPSC amplitude analysis during repetitive stimulation (60 Hz, 60 stimuli; see Material & Methods) (Fig. 3B). Cumulative EPSC amplitudes in the absence and presence of Gyki showed no statistically significant difference, analogous to PhTx treatment (Fig. 3C). In combination with the receptor perturbation-induced decrease in mEPSP amplitude (Fig. 3A), this translated into a significant increase in cumulative apparent quantal content (cum. EPSC/mEPSP) and apparent RRP size (back-extrapolated cum. quantal content at y-intercept) upon receptor inhibition (Fig. 3C). Thus, Gyki treatment augments RRP size, similar to PhTx.

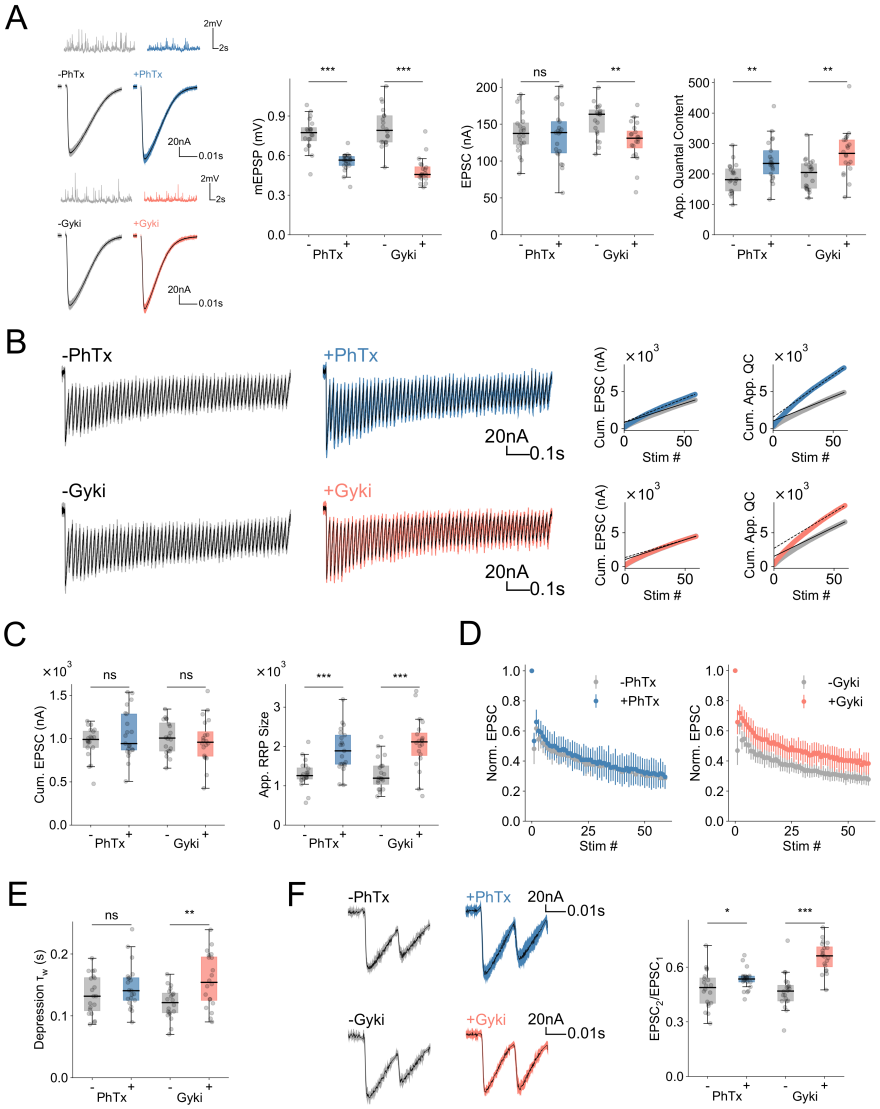

*Fig 3. Both Gyki and PhTx increase RRP size, but with differences in short-term plasticity. (**A**) Representative traces (mEPSPs and EPSCs), mEPSP amplitudes, EPSC amplitudes and apparent quantal content (EPSC/mEPSP) of PhTx-untreated or treated, as well as Gyki-untreated or treated NMJs. Both PhTx and Gyki treatment increased apparent quantal content. n = 20 (-PhTx) vs 21 (+PhTx); n = 20 (-Gyki) vs 20 (+Gyki). $[Ca^{2+}]_e$ = 1.0 mM. (**B**) Representative EPSC trains (60 stimuli at 60 Hz frequency), cumulative EPSC, cumulative apparent quantal content (cumulative EPSC/mEPSP) from PhTx-untreated or treated, and Gyki-untreated or treated NMJs. Cumulative EPSC and cumulative apparent quantal content are plotted as a function of stimulus number. $[Ca^{2+}]_e$ = 1.0 mM. (**C**) Cumulative EPSC (y-intercept obtained by fitting the last 10 points of the cumulative EPSC), and apparent RRP size (Cumulative EPSC/mEPSP amplitude) of PhTx-untreated or treated, and Gyki-untreated or treated NMJs. Both, PhTx and Gyki treatment result in an increase in apparent RRP size. (**D**) Normalized EPSC amplitudes of all NMJs for PhTx-untreated or treated, and Gyki-untreated or treated experimental groups. Error bars represent standard deviation. (**E**) Weighted depression time constant of normalized EPSC amplitudes (τ_w) of PhTx- untreated or treated, and Gyki-untreated or treated NMJs. (**F**) Paired-pulse ratio ($EPSC_2/EPSC_1$) of PhTx-untreated or treated, and Gyki-untreated or treated NMJs. Pairwise comparisons were done with a two-sided Mann Whitney U test. Each data point indicates the median value for a given cell. ns : p >= 0.05; * : p < 0.05; ** : p < 0.01; *** : p < 0.001.*

Although both, Gyki and PhTx treatment increased RRP size, we observed differences in short-term dynamics of EPSC amplitudes during the trains between the two conditions (Fig. 3D). We first compared the depression time course during the trains between control and treated NMJs, as quantified by a weighted time constant (τ_w) of a double-exponential fit to the normalized EPSC amplitudes during the train (see Material & Methods). While the depression time course was similar between control and PhTx-treated NMJs (Fig. 3D, E), there was a significant increase in the median τ_w after Gyki application (Fig. 3D, E), implying a decelerated depression time course. Moreover, the train responses also indicated a substantial (~40%) increase in paired-pulse ratio (PPR) between the second and the first EPSC amplitudes ($EPSC_2/EPSC_1$) after Gyki application (Fig. 3F). By contrast, the PPR was only marginally (~8%) increased upon PhTx treatment (Fig. 3F). These results establish that Gyki treatment attenuates synaptic depression, indicative of a reduction in release probability or changes in receptor properties (see Discussion). PhTx, on the other hand, does not result in apparent changes in short-term plasticity.

Together, we conclude that Gyki and PhTx treatment increase RRP size with different effects on short-term plasticity.

PhTx, but not Gyki, upregulates Brp abundance

We next asked whether the homeostatic modulation of active zone proteins is differentially affected by Gyki and PhTx treatment (Fig. 4). Several studies revealed increased immunofluorescence intensity of several active zone proteins upon PhTx application at the *Drosophila* NMJ, including the scaffolding protein bruchpilot (Brp) (Böhme et al., 2019; Gratz et al., 2019; Weyhersmuller et al., 2011). We therefore tested if Gyki application affects Brp abundance. To this end, we immunostained Brp and imaged after incubation with saline, PhTx or Gyki for ~15 minutes using confocal microscopy (Fig. 4A; see Material & Methods). At confocal resolution, Brp forms punctated structures (Kittel et al., 2006) (Fig. 4A). After PhTx treatment, we detected a small, but statistically significant increase in Brp fluorescence intensity (Fig. 4B), as reported previously (Weyhersmuller et al., 2011). On the other hand, we did not observe any increase in Brp intensity after Gyki treatment (Fig. 4B). On the contrary, Brp fluorescence intensity was even lower at Gyki-treated NMJs compared to control or PhTx-treated NMJs (Fig. 4B). Considering a positive relationship between Brp abundance and release probability (Kittel et al., 2006), this observation would be consistent with the electrophysiology data indicating reduced release probability upon Gyki treatment (Fig. 3), and the additional release of a low-release probability vesicles during PHP (Wentzel et al., 2018). Hence, although both PhTx and Gyki inhibit GluRs and induce PHP, only PhTx leads to an increase in Brp abundance/density, supporting the idea that receptor perturbation by these two antagonists triggers different molecular pathways.

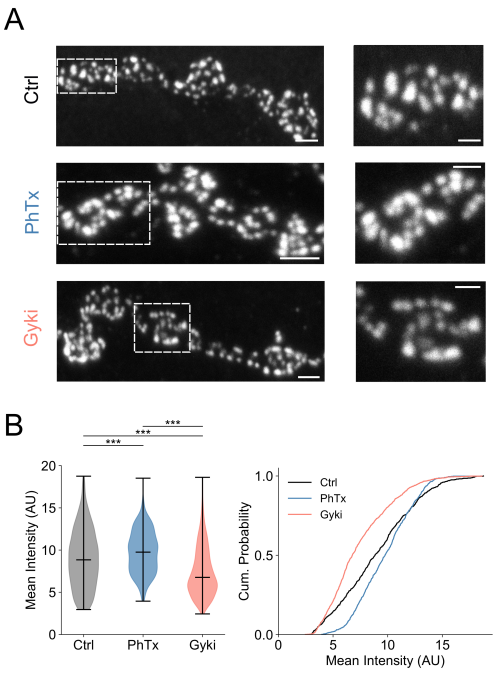

*Fig 4. PhTx and Gyki exhibit differences in Brp regulation. (**A**) Representative confocal images (max. intensity projection) of anti-Brp stained NMJs, treated with saline (Ctrl), PhTx or Gyki. Right column displays the enlarged view of the boxed regions. Scale bars: 2 µm for NMJs, and 1 µm for the enlarged view. (**B**) Quantified mean intensities for saline, PhTx or Gyki treated NMJs. Number of active zones, n: 617 (Ctrl), 749 (PhTx), and 1114 (Gyki). Number of NMJs: 7 (Ctrl), 6 (PhTx), and 8 (Gyki). Statistical significance was assessed using a Kruskal-Wallis test (the obtained p value was < 0.001), followed by Dunn's post hoc comparison. ns : p >= 0.05; * : p < 0.05; ** : p < 0.01; *** : p < 0.001.*

Gyki induces PHP at mutant NMJs with impaired PhTx-induced PHP

The observation of differential Brp modulation in response to Gyki and PhTx treatment indicates that these two antagonists may induce PHP via distinct molecular mechanisms. Electrophysiology-based genetic screens in *Drosophila* have identified several genes involved in PhTx-induced PHP (Delvendahl and Müller, 2019). If PHP is indeed driven by distinct molecular mechanisms in response to Gyki and PhTx treatment, then Gyki may induce PHP in a genetic background that blocks PhTx-induced PHP.

We first tested PHP in RIM loss of function mutants, $rim^{\Delta 103}$, which were shown to have disrupted PhTx-induced PHP (Muller et al., 2012). PhTx application reduced the median mEPSP amplitude and the median EPSP amplitude by a similar degree at $rim^{\Delta 103}$ mutant NMJs (Fig. 5A). Correspondingly, quantal content remained unchanged after PhTx application (Fig. 5A), indicating impaired PhTx-induced PHP,

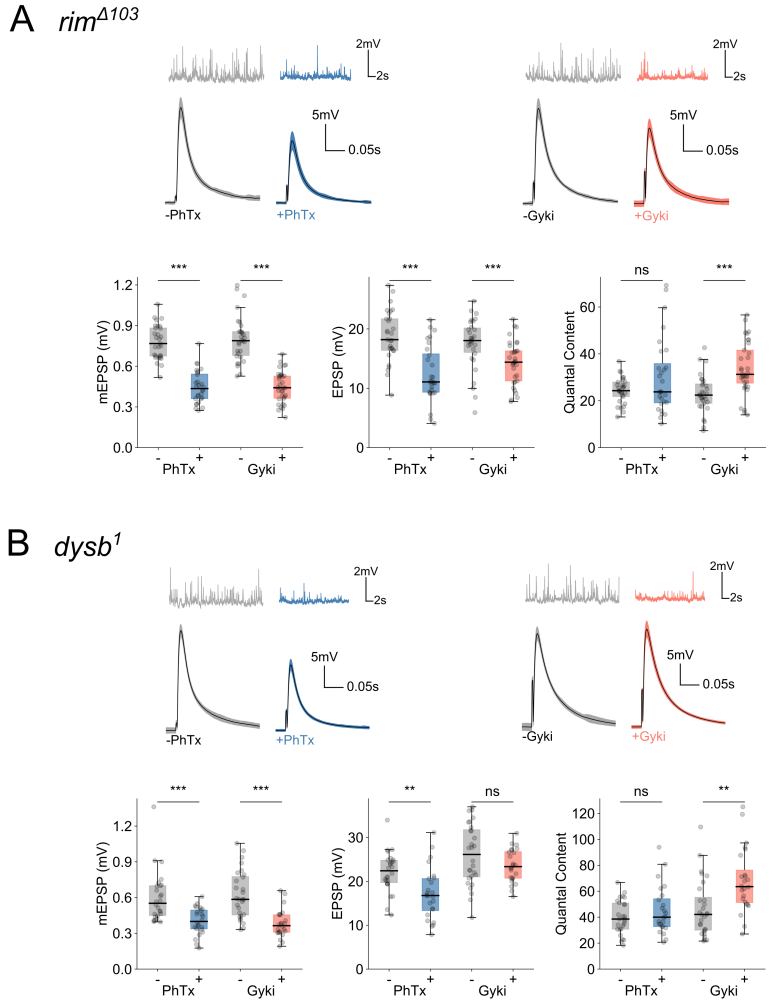

consistent with previous work (Muller et al., 2012). Similar to PhTx treatment, Gyki application decreased the median mEPSP amplitude by >50% compared to untreated *rim*$^{\Delta 103}$ NMJs (Fig. 5A). By contrast, the median EPSP amplitude was reduced by only ~20% upon Gyki treatment (Fig. 5A), translating into a significant increase in quantal content (Fig. 5A). Thus, Gyki application increases quantal content in *rim*$^{\Delta 103}$ mutants, suggesting PHP expression.

Next, we probed PHP after loss of *dysbindin* (*dysb*), a gene implicated in PhTx-induced PHP by several studies (Dickman and Davis, 2009; Wentzel et al., 2018). Both, PhTx and Gyki treatment significantly reduced mEPSP amplitudes in *dysb*^{1} mutants (Fig. 5B). While EPSP amplitudes were significantly decreased upon PhTx application, they remained unaffected at Gyki-treated NMJs (Fig. 5B). Consequently, quantal content was unchanged after PhTx application, but enhanced after Gyki treatment (Fig. 5B). Hence, PHP is blocked in *dysb*^{1} mutants after PhTx, but not after Gyki application. This implies that *dysb* is not involved in Gyki-induced PHP, but required for PhTx-induced PHP. Together, the analysis of *rim* and *dysb* mutants suggests that PhTx and Gyki-induced PHP involve distinct molecular mechanisms.

*Fig 5. Gyki induces PHP at mutant NMJs with impaired PhTx-induced PHP. (**A**) Representative traces (mEPSPs and EPSPs), mEPSP amplitudes, EPSP amplitudes, and quantal content for PhTx-untreated or treated, and Gyki-untreated or treated rim mutant NMJs. PhTx treatment does not affect quantal content, indicating impaired PhTx-induced PHP. On the other hand, Gyki treatment results in PHP, as indicated by increased quantal content. n = 29 (-PhTx) vs 28 (+PhTx); n = 30 (-Gyki) vs 33 (+Gyki). $[Ca^{2+}]_e$ = 0.4 mM. (**B**) Representative traces (mEPSPs and EPSPs), mEPSP amplitudes, EPSP amplitudes, and quantal content for PhTx-untreated or treated, and Gyki-untreated or treated dysb mutant NMJs. PhTx treatment does not affect quantal content, indicating impaired PhTx-induced PHP. On the other hand, Gyki treatment results in PHP, as indicated by increased quantal content. n = 26 (-PhTx) vs 24 (+PhTx); n = 28 (-Gyki) vs 24 (+Gyki). $[Ca^{2+}]_e$ = 0.4 mM. Pairwise comparisons were done with a two-sided Mann Whitney U test. Each data point indicates the median value for a given cell. ns : p >= 0.05; * : p < 0.05; ** : p < 0.01; *** : p < 0.001.*

Besides postsynaptic GluRs, the *Drosophila* NMJ also expresses presynaptic kainate receptors (DKaiR1D) that are required for PhTx-induced PHP (Kiragasi et al., 2017). In principle, one reason for the apparent differences between PHP induced by PhTx and Gyki application could be that Gyki may induce PHP by directly acting on presynaptic DKaiR1D receptors, rather than postsynaptic GluRs. However,

Gkyi-induced PHP proceeds normally in *DKaiR1D* null mutants (*KaiR1D*^{2}; (Kiragasi et al., 2017)) (Fig. S1), implying that Gyki does not induce PHP via presynaptic kainate receptors. By extension, this finding provides further evidence for distinct molecular pathways underlying PhTx- and Gyki-induced PHP.

Presynaptic Protein Kinase D promotes Gyki-induced PHP, but not PhTx-induced PHP

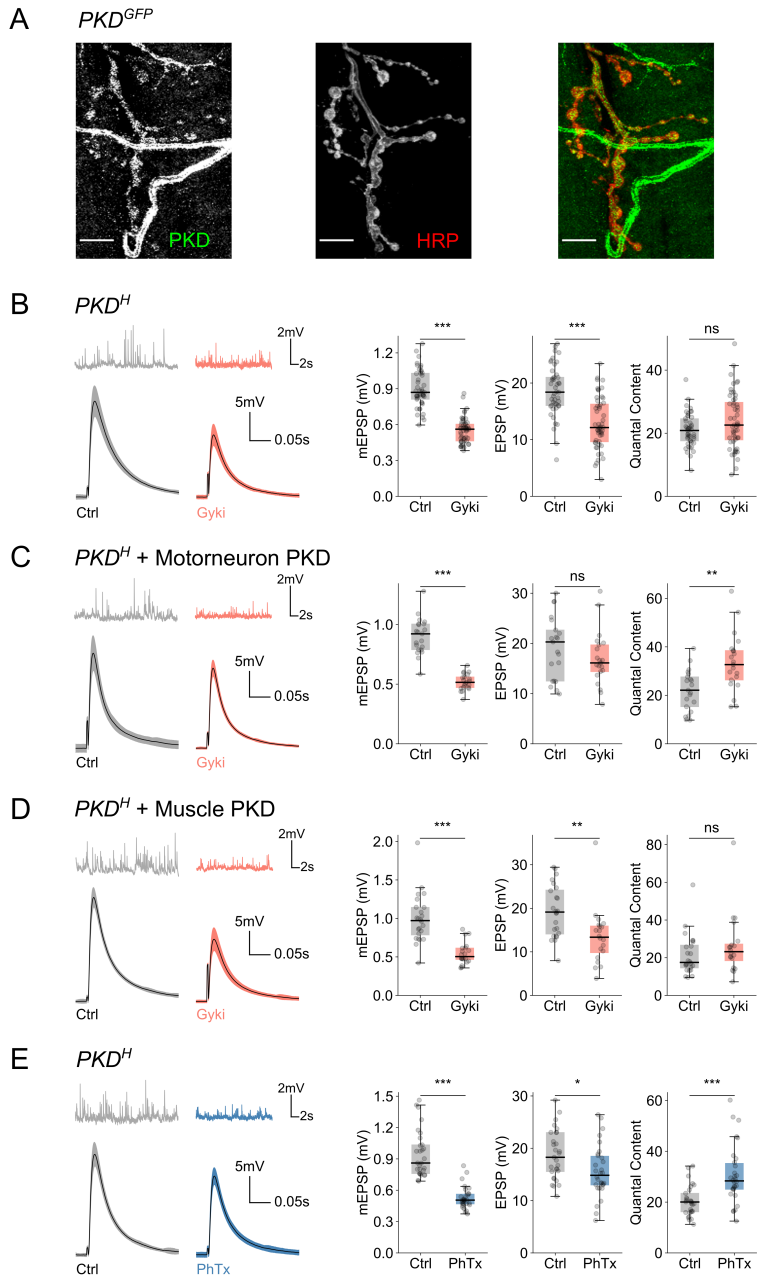

*Fig 6. Presynaptic PKD promotes Gyki-induced PHP, but not PhTx-induced PHP. (**A**) Expression of fluorescently-tagged endogenous PKD (stained with anti-GFP) and the neuronal membrane marker HRP. PKD fluorescence (green) overlaps with HRP (red) in the merged image. In addition, PKD expression was seen in other non-neuronal compartments, such as trachea. Scale bar = 10 µm. (**B**) Representative traces (mEPSPs and EPSPs), mEPSP amplitudes, EPSP amplitudes and quantal content of saline (Ctrl) or Gyki-treated hypomorphic PKD^{H} mutant NMJs. There was no increase in quantal content after Gyki treatment, indicating impaired Gyki-induced PHP. n = 45 (Ctrl) vs 52 (Gyki). $[Ca^{2+}]_e$ = 0.3 mM. (**C**) Representative traces (mEPSPs and EPSPs), mEPSP amplitudes, EPSP amplitudes and quantal content of saline (Ctrl) or Gyki-treated NMJs expressing wild-type PKD in motorneurons of PKD^{H} mutants. Quantal content increased in the presence of Gyki, indicating PHP induction in response to Gyki. n = 21 (Ctrl) vs 21 (Gyki). $[Ca^{2+}]_e$ = 0.3 mM. (**D**) Representative traces (mEPSPs and EPSPs), mEPSP amplitudes, EPSP amplitude and quantal content of saline (Ctrl) or Gyki-treated NMJs expressing wild-type PKD in postsynaptic muscles of PKD^{H} mutants. There was no increase in quantal content after Gyki treatment, indicating impaired Gyki-induced PHP. n = 24 (Ctrl) vs 20 (Gyki). $[Ca^{2+}]_e$ = 0.3 mM. (**E**) Representative traces (mEPSPs and EPSPs), mEPSP amplitudes, EPSP amplitude and quantal content of saline (Ctrl) or PhTx treated PKD^{H} mutant NMJs. Quantal content increased after PhTx treatment, indicating PHP induction in response to PhTx. n = 29 (Ctrl) vs 30 (PhTx). $[Ca^{2+}]_e$ = 0.3 mM. Pairwise comparisons were done with a two-sided Mann Whitney U test. Each data point indicates the median value for a given cell. ns : p >= 0.05; * : p < 0.05; ** : p < 0.01; *** : p < 0.001.*

We next carried out a small, targeted genetic screen to identify molecular players involved in Gyki-induced PHP. This screen revealed that a MiMIC transposon insertion upstream of the *Protein Kinase D* (*PKD*) locus, henceforth called *PKD*^{H}, blocks PHP in response to Gyki treatment. *PKD*^{H} is a hypomorphic allele with strongly reduced (up to 70%) PKD transcript levels (Ashe et al., 2018). Although *Drosophila* PKD shows a broad expression pattern (Maier et al., 2006), its presence at the NMJ remains unclear. Therefore, we analyzed PKD expression at the larval body wall of third instar larvae using fluorescently-tagged endogenous PKD

(*PKD*^{GFP}) generated from an intronic MiMIC insertion in the *PKD* gene (Nagarkar-Jaiswal et al., 2015). This analysis revealed PKD fluorescence in various compartments, including motorneurons, muscles and trachea (Fig. 6A). PKD fluorescence was particularly enriched in close proximity to the neural membrane marker horseradish peroxidase (HRP), demonstrating PKD expression in neurons and the synaptic compartments (Fig. 6A). In the context of PHP, Gyki application significantly reduced mEPSP and EPSP amplitudes by a similar magnitude in *PKD*^{H} mutants (Fig. 6B). Correspondingly, there was no increase in quantal content in *PKD*^{H} mutants (Fig. 6B), indicating impaired PHP. We did not detect any gross morphological changes in synaptic organization in *PKD*^{H} mutants (Fig. S2A), implying that the PHP defect is unlikely a secondary consequence of impaired synaptic development.

We next asked whether PKD acts presynaptically or postsynaptically during PHP employing cell-type specific rescue experiments. First, we tested a potential presynaptic involvement of PKD in PHP by motorneuron-specific (*OK371-Gal4*) expression of a wild-type *PKD* transgene (*UAS-PKD*^{WT}, (Maier et al., 2007)) in the *PKD*^{H} mutant background. As expected, Gyki application resulted in a significant decrease in mEPSP amplitudes (Fig. 6C). However, unlike in the case of *PKD*^{H}, there was no reduction in EPSP amplitudes, translating into a significant increase in quantal content, indicating robust PHP expression (Fig. 6C). On the other hand, Gyki application did not result in any quantal content increase after muscle-specific (*Mef2-Gal4*) *PKD* expression in *PKD*^{H} mutants, implying PHP disruption (Fig. 6D). Thus, presynaptic, but not postsynaptic *PKD* expression restores PHP in the *PKD*^{H} mutant background. By extension, the restoration of PHP upon presynaptic *PKD* expression indicates that PHP disruption in *PKD*^{H} mutants is not a secondary effect of PKD loss in other cell types. We further confirmed a presynaptic role for PKD in PHP by motorneuron (*D42-Gal4*) or muscle-specific (*Mef2-Gal4*) expression of *UAS-PKD*^{RNAi}. Consistent with the rescue experiments, we observed that neural, but not muscle-specific *PKD*^{RNAi} expression disrupted PHP (Fig. S2B, C). Together, these results demonstrate a presynaptic role for PKD in the context of Gyki-induced PHP.

Finally, we investigated whether PKD is also involved in PhTx-induced PHP by probing synaptic responses of *PKD*^{H} mutant NMJs after PhTx application (Fig. 6E). PhTx decreased mEPSP amplitude by ~40% in *PKD*^{H} mutants (Fig. 6E). However, EPSP amplitudes were only reduced by ~20% (Fig. 6E), translating into a significant increase in quantal content (Fig. 6E). Hence, PhTx treatment in *PKD*^{H} mutants results in an increase in quantal content, suggesting that PKD is largely dispensable for PhTx-induced PHP expression. This differential requirement of PKD for Gyki- and PhTx-induced PHP further supports the notion that Gyki and PhTx induce PHP via distinct molecular mechanisms.

Discussion

We here discovered that distinct mechanisms underlie PHP induced by the allosteric GluR antagonist Gyki-53655 and the pore-blocker PhTx-433. This involved differential modulation of the active-zone protein Brp and short-term plasticity during PHP induced by these two antagonists. Importantly, we provide genetic evidence that separable molecular mechanisms promote PHP in response to Gyki and PhTx treatment. On the other hand, the competitive GluR antagonist γDGG did not produce PHP despite a robust reduction in postsynaptic receptor function. Together, our data suggest that distinct molecular mechanisms mediate PHP in response to different types of pharmacological GluR inhibition, and that GluR inhibition *per se* is not sufficient for PHP expression.

Prevalent models of homeostatic synaptic plasticity rest on the assumption that synaptic activity changes induce homeostatic signaling (Frank et al., 2006; Turrigiano, 2008). In the case of PHP, the magnitude of the homeostatic increase in presynaptic release scales with the decrease in the amplitude of postsynaptic miniature events (Frank et al., 2006). Based on these data, it was proposed that reduced ion flux through the receptors triggers a homeostatic signaling cascade in the postsynaptic cell, which is relayed to the presynaptic compartment where it adjusts release. A prediction that directly follows is that

any receptor perturbation with similar effects on ion flux through the receptor produces the same homeostatic response via similar underlying mechanisms. We observed that two GluR antagonists, PhTx and Gyki, induced PHP, while one antagonist, γDGG did not. All three perturbations had similar effects on ion flux through the receptors, observed as changes in quantal size. Although we cannot exclude the possibility that γDGG may have directly blocked PHP expression, our results suggest that ion flux is unlikely the sole signal responsible for PHP induction at the *Drosophila* NMJ. Possibly, some additional parameters, besides ion flux, are also sensed by the downstream signaling to induce homeostasis. This agrees with recent observations at the *Drosophila* and mouse NMJ that Ca^{2+} flux through the receptor is likely dispensable for PHP induction (Goel et al., 2017; Wang et al., 2018).

Although we did not test competitive GluR antagonists other than γDGG, one intriguing possibility is that competition with glutamate binding may have blocked PHP induction upon γDGG treatment. As ligand binding constitutes the activation signal for the receptor, competitive inhibition essentially dampens the input signal itself. Thus, competitive GluR inhibition by γDGG may mimic a scenario of reduced receptor activation or a period of quiescence, rather than receptor perturbation. On the other hand, the pore-blocker PhTx and the allosteric antagonist Gyki could signal perturbation, because they reduce receptor function despite the receptor receiving activation signals in the form of glutamate binding. Validation of such a scenario requires further investigation.

In contrast to γDGG, both PhTx and Gyki application induced robust PHP within minutes through an increase in RRP size. However, we observed several differences between PhTx- and Gyki-induced PHP: First, while Gyki treatment reduced short-term depression, short-term plasticity was largely unchanged after PhTx application. This change in short-term plasticity indicates that Gyki application may potentiate the release of low release probability vesicles more potently than PhTx (Wentzel et al., 2018). Alternatively, both antagonists may differentially affect GluRs during repetitive stimulation. Second, we observed that PhTx treatment increased Brp abundance, whereas Gyki did not. This implies that PhTx- and Gyki-induced PHP involve separable molecular mechanisms. Instead, we even detected a slight decrease in Brp abundance upon Gyki treatment. Given the correlation between Brp levels and release probability (Kittel et al., 2006), this finding would be in line with the reduced release probability after Gyki application, and the additional recruitment of a low-release probability pool during PHP reported previously (Wentzel et al., 2018). Third, the notion of distinct molecular mechanisms is further supported by our genetic data, which showed that PHP in response to Gyki and PhTx treatment require different genes. Gyki-induced PHP proceeds normally in two mutants, which were previously shown to block PHP upon PhTx treatment (*dysbindin* and *rim*, (Dickman and Davis, 2009; Muller et al., 2012)). Additionally, we discovered the first gene (*PKD*) that is required for PHP in response to Gyki application, but not PhTx treatment. Thus, although we cannot exclude the possibility of partially overlapping molecular mechanisms, these data demonstrate separable molecular pathways.

The function of PKD in synaptic transmission or synaptic plasticity is largely unknown. Recent investigations have implicated PKD in F-actin stabilization in dendritic spines, learning and memory (Oueslati Morales et al., 2020), or the regulation of AMPAR endocytosis and chemically-induced long-term depression (Oueslati Morales et al., 2020). By contrast, little is known about its role in regulating presynaptic function. PKD has been linked to various intracellular processes, such as vesicle sorting (Baron and Malhotra, 2002), endocytosis (Ellwanger and Hausser, 2013), and regulation of the actin cytoskeleton (Olayioye et al., 2013), which are also important for synaptic function.

Diverging homeostatic signaling has been observed in the context of acute versus chronic receptor perturbations. At the *Drosophila* NMJ, mutants that exhibited acute PHP in response to PhTx application displayed PHP block in the chronic *GluRIIC* mutant background condition (James et al., 2019). Moreover, PHP during chronic GluR perturbation involves increased recruitment of low release probability vesicles compared to acute PHP induced by PhTx (Genç and Davis, 2019). Since our experiments focus on acute perturbations, our analysis is largely restricted to the effects of different types of receptor perturbations rather than different perturbation timescales. Differential signaling has also been

observed in the context of firing rate homeostasis, where molecular responses depend on whether a sodium channel protein or channel conductance is eliminated (Kulik et al., 2019). Thus, distinct molecular signaling specific to the molecular nature, rather than the functional effects of perturbations, may be a general theme in the context of neuronal homeostasis.

There are two important questions that emerge from our data. How could pharmacological receptor perturbation induce PHP independent of ion flux through the receptor? And, why does PHP in response to PhTx and Gyki engage different signaling? One intriguing possibility is that perturbation-specific conformational changes of the receptor may be involved in PHP signaling (Goel et al., 2017; Wang et al., 2018). Conformational changes of kainate-, AMPA- and NMDA-type GluRs at mammalian synapses are known to signal independent of ion flux in the context of synaptic plasticity, possibly through metabotropic signaling (Valbuena and Lerma, 2016). It is also known that different antagonists stabilize different conformational states of AMPA receptors (Balannik et al., 2005; Twomey et al., 2018). Thus, it is conceivable that distinct antagonists may trigger different signaling depending on the specific conformational state. However, direct evidence for this hypothesis remains sparse. Our indirect evidence for non-canonical, possibly metabotropic, GluR signaling during PHP in the genetic model organism *Drosophila* presents a starting point to investigate the molecular mechanisms underlying non-canonical GluR signaling.

Unlike PhTx (Frank et al., 2006), Gyki induced PHP in the fully dissected NMJ preparation, which is more amenable to electrophysiology and imaging approaches. The fact that Gyki results in PHP after full dissection demonstrates that PHP induction is not limited to the “semi-intact” preparation *per se*. Furthermore, the possibility to induce PHP in a fully dissected preparation will facilitate real-time monitoring and further characterization of PHP induction. Gyki also allows studying the molecular mechanisms promoting PHP reversibility at the *Drosophila* NMJ, because it blocks GluRs reversibly, unlike PhTx (Frank et al., 2006). PHP reversed within minutes after Gyki washout, similar to Gyki washout at cerebellar mossy fiber bouton to granule cell synapses (Delvendahl et al., 2019), or D-Tubocurarine washout at the mouse NMJ (Wang et al., 2016), and much faster than the reversal of genetic GluR perturbation at the *Drosophila* NMJ (2 – 3 days) (Yeates et al., 2017).

In general, different perturbations are interchangeably used to study a given form of homeostatic plasticity. For example, in the context of PHP, pharmacological and genetic manipulations of different receptor subunits are often viewed as equivalent experimental perturbations. Based on our finding of perturbation-specific homeostatic signaling, future experiments should consider the exact nature of a perturbation used to study homeostatic plasticity. Even in cases where different perturbations result in similar homeostatic compensation, there may be differences in the underlying signaling pathways.

Materials and Methods

Fly Stocks

Drosophila stocks were raised at 25°C on normal molasses-containing food. The following genotypes were used: w^{1118} served as wildtype, *Mef2-Gal4* (kind gift from Monica Zwicky's lab, University of Zurich, Switzerland), *D42-Gal4* (Bloomington Drosophila Stock Center - 8816), *OK371-Gal4* (Bloomington Drosophila Stock Center - 26160), $dysb^{1}$, $rim^{\Delta 103}$, PKD^{H} ($PKD^{MI03619}$; Bloomington Drosophila Stock Center - 37604), PKD^{GFP} ($PKD^{MI09308\text{-}GFSTF.0}$; Bloomington Drosophila Stock Center - 60273), *UAS-PKD-RNAi* (TRiP.HMC04179; Bloomington Drosophila Stock Center - 55898), *UAS-*PKD^{WT} (kind gift from Anette Preiss' lab, University of Hohenheim, Germany). The *Mef2-Gal4* driver line was used for muscle-specific expression and either *D42-Gal4* or *OK371-Gal4* was used for motor-neuron expression.

Electrophysiology

Wandering third-instar larvae were dissected in HL3 solution (5 mM KCl, 70 mM NaCl, 10 mM Na-HEPES, 5 mM HEPES, 5 mM trehalose, 115 mM sucrose, 10 mM $MgCl_2$) with 0.3 mM $CaCl_2$ for sharp-electrode membrane voltage recordings (unless stated otherwise), or 1.0 mM $CaCl_2$ for two-electrode voltage clamp (TEVC) recordings. The internal organs, including brain and ventral nerve cord, were carefully removed from the body-wall with intact muscle fibers and innervating motor nerves. Sharp-electrode and TEVC recordings were performed on muscle 6 of segments 3 and 4 with sharp glass electrodes (resistance 10-25 MΩ) using an Axoclamp 900A amplifier (Molecular Devices) and a combination of HS 9A x0.1 and HS 9A x10 headstages. For TEVC recordings, muscle cells were clamped to a membrane potential of −65 mV. For individual NMJs, mEPSPs were recorded prior to EPSP/Cs induced by stimulating the respective hemi-segmental nerve with single APs (3 ms or 0.3 ms stimulus duration for EPSPs and EPSCs, respectively, 0.3 Hz). A total of 50 EPSCs or 30 EPSPs were recorded to obtain the median EPSC or EPSP value, respectively, for each cell.

For the experiments in Fig. 1, semi-intact (dorsally dissected; with internal organs, brain and ventral nerve cord intact) larvae were incubated with GluR antagonist for ~15 minutes. This was followed by removal of internal organs, brain and ventral nerve cord to obtain a fully-stretched preparation for electrophysiological recordings. Recordings for γDGG and Gyki were performed in the presence of respective inhibitors. For PhTx, we used the previously described protocol in which PhTx was thoroughly washed out with HL3 after the removal of internal organs, brain and ventral nerve cord (Frank et al., 2006). Due to the irreversible binding of PhTx, a significant fraction of receptors remains inhibited after washout. The following inhibitor concentrations were used: PhTx (20 μM; Cat # sc-255421, Santa Cruz Biotechnology), Gyki (10 μM; Cat # 2555, Tocris) and γDGG (5 mM; Cat # 0112, Tocris). Except for experiments in Fig. 1, all experiments with Gyki were performed by directly applying Gyki to the fully stretched larval preparation. For PHP reversibility experiments, fully-stretched larval preparations were incubated with either Gyki or HL3 for ~15 minutes followed by a wash with HL3 and a further incubation with HL3 for ~15 minutes before electrophysiological recordings.

Immunohistochemistry

Third-instar larvae were dissected in HL3 and fixed for 10 minutes in 100% ice-cold ethanol followed by rinsing 3 times with PBS. Larvae were washed afterwards 5x 10 minutes with PBS and 0.1% PBT on a rotating wheel. This was followed by 2 hours blocking with 3% normal goat serum in PBT, before incubating the samples with primary antibodies at 4°C overnight. Larvae were washed 5x 10 min with PBT on the following day and then incubated with secondary antibodies in blocking solution for ~2 hour.

This was followed by 5x 10 min wash with PBT before mounting on glass slides with ProLong Gold Antifade (Thermo Fisher Scientific). The following primary antibodies were used: anti-Brp (mouse, nc82; 1:100), anti-Disc large (rabbit, DSHB AB_2617529; 1:10000), anti-GFP (mouse, Life Technologies 3E6; 1:1000) and Alexa-677 conjugated anti-HRP. The following secondary antibodies were used: Alexa-488 conjugated anti-mouse (Life Technologies A11029; 1:100), Alexa-555 conjugated anti-rabbit (Life Technologies A21429; 1:100), and Atto594 conjugated anti-mouse (ATTO-TEC; 1:100). Images were acquired using an inverted Leica SP8 laser scanning microscope (University of Zurich Center for Microscopy and Image Analysis) controlled with LASX software suite (Leica Microsystems, Germany). For Brp intensity quantification imaging, excitation light (580nm or 640nm) of a flexible white light laser was focused onto the specimen using a 100x objective (HC PL APO 1.40 NA Oil STED WHITE; Leica Microsystems, Germany) with immersion oil conforming to ISO 8036 with a diffraction index of n=1.5180 (Leica Microsystems, Germany). Emitted light was detected with two HyD detectors in photon counting mode (Leica Microsystems, Germany). Pixel size was 20 x 20 nm and z-stacks were acquired with a step size of 120 nm.

Data Analysis

Electrophysiology data were analyzed using routines written with scientific python libraries, including numpy, scipy, IPython and neo (Garcia et al., 2014). mEPSP events were detected using a template-matching algorithm (Clements and Bekkers, 1997). Quantal content for current-clamp recordings were calculated as the ratio of the median EPSP amplitude and the median mEPSP amplitude for a given cell. We used the ratio between EPSC amplitude and mEPSP amplitude to calculate “apparent quantal content”, because the low signal-to-noise ratio of TEVC recordings at high clamp gain does not permit reliable mEPSC detection.

The readily releasable pool (RRP) size was estimated by the method of back-extrapolation of cumulative EPSC amplitudes measured during stimulus trains (Schneggenburger et al., 1999). Briefly, presynaptic nerve terminals were stimulated with 60 stimuli at 60 Hz and EPSCs were recorded. The cumulative EPSC amplitudes were then plotted as a function of stimulus number. The last 10 cumulative EPSC amplitudes were fitted with a straight line, and this line was extrapolated to the y-axis intercept. The y-intercept indicates the total response produced by RRP. “Apparent RRP” was estimated as the ratio of the y-intercept and the median mEPSP amplitude from the same cell. We used the term “apparent RRP”, because cumulative EPSC amplitudes were normalized by mEPSP amplitudes (see above). The weighted time constant (τ_w) for the train response was estimated by fitting the normalized EPSC amplitudes during the train with a double exponential function (a_1*exp(-t/τ_1) + a_2*exp(-t/τ_2)). τ_w was then estimated using the fitted double exponential function parameters, (a_1*τ_1 + a_2*τ_2)/(a_1 + a_2).

Microscopy images were analyzed using custom routines written in ImageJ (version 1.51n, National Institutes of Health, USA). Brp fluorescence intensity quantification was performed as follows: First individual Brp puncta were isolated by segmenting binary threshold masks (15% or 35% of the maximum intensity value), background corrected (rolling ball, radius = 1 µm) and filtered (3 x 3 median) maximum intensity projection images. Average intensity values were then calculated for each Brp puncta from raw maximum intensity projection images.

Statistical Analysis

Statistical tests were performed using the stats module of scipy and scikit-posthocs. Two-sided Mann-Whitney U Tests were used to perform statistical comparison, and for multiple data comparison, a Kruskal-Wallis test followed by Dunn’s post hoc comparison was performed.

References

Ashe, S., Malhotra, V., and Raghu, P. (2018). Protein kinase D regulates metabolism and growth by controlling secretion of insulin like peptide. Dev. Biol. *434*, 175–185.

Balannik, V., Menniti, F.S., Paternain, A. V, Lerma, J., and Stern-Bach, Y. (2005). Molecular mechanism of AMPA receptor noncompetitive antagonism. Neuron *48*, 279–288.

Baron, C.L., and Malhotra, V. (2002). Role of diacylglycerol in PKD recruitment to the TGN and protein transport to the plasma membrane. Science *295*, 325–328.

Böhme, M.A., McCarthy, A.W., Grasskamp, A.T., Beuschel, C.B., Goel, P., Jusyte, M., Laber, D., Huang, S., Rey, U., Petzoldt, A.G., et al. (2019). Rapid active zone remodeling consolidates presynaptic potentiation. Nat. Commun. *10*, 1–16.

Clements, J.D., and Bekkers, J.M. (1997). Detection of spontaneous synaptic events with an optimally scaled template. Biophys. J. *73*, 220–229.

Delvendahl, I., and Müller, M. (2019). Homeostatic plasticity—a presynaptic perspective. Curr. Opin. Neurobiol. *54*, 155–162.

Delvendahl, I., Kita, K., and Müller, M. (2019). Rapid and sustained homeostatic control of presynaptic exocytosis at a central synapse. Proc. Natl. Acad. Sci. U. S. A. *8057*, 1–7.

Dickman, D.K., and Davis, G.W. (2009). The schizophrenia susceptibility gene dysbindin controls synaptic homeostasis. Science *326*, 1127–1130.

Ellwanger, K., and Hausser, A. (2013). Physiological functions of protein kinase D in vivo. IUBMB Life *65*, 98–107.

Frank, C.A., Kennedy, M.J., Goold, C.P.P., Marek, K.W., and Davis, G.W.W. (2006). Mechanisms Underlying the Rapid Induction and Sustained Expression of Synaptic Homeostasis. Neuron *52*, 663–677.

Garcia, S., Guarino, D., Jaillet, F., Jennings, T., Pröpper, R., Rautenberg, P.L., Rodgers, C.C., Sobolev, A., Wachtler, T., Yger, P., et al. (2014). Neo: An object model for handling electrophysiology data in multiple formats. Front. Neuroinform. *8*, 1–10.

Genç, Ö., and Davis, G.W. (2019). Target-wide Induction and Synapse Type-Specific Robustness of Presynaptic Homeostasis. Curr. Biol. *29*, 3863–3873.

Genç, Ö., An, J.Y., Fetter, R.D., Kulik, Y., Zunino, G., Sanders, S.J., and Davis, G.W. (2020). Homeostatic plasticity fails at the intersection of autism-gene mutations and a novel class of common genetic modifiers. Elife *9*, 1–32.

Goel, P., Li, X., and Dickman, D. (2017). Disparate Postsynaptic Induction Mechanisms Ultimately Converge to Drive the Retrograde Enhancement of Presynaptic Efficacy. Cell Rep. *21*, 2339–2347.

Gratz, S.J., Goel, P., Bruckner, J.J., Hernandez, R.X., Khateeb, K., Macleod, G.T., Dickman, D., and O'Connor-Giles, K.M. (2019). Endogenous tagging reveals differential regulation of Ca2+ channels at single active zones during presynaptic homeostatic potentiation and depression. J. Neurosci. *39*, 2416–2429.

Ibata, K., Sun, Q., and Turrigiano, G.G. (2008). Rapid synaptic scaling induced by changes in postsynaptic firing. Neuron *57*, 819–826.

James, T.D., Zwiefelhofer, D.J., and Frank, C.A. (2019). Maintenance of homeostatic plasticity at the drosophila neuromuscular synapse requires continuous IP3-directed signaling. Elife *8*, 1–28.

Keck, T., Keller, G.B., Jacobsen, R.I., Eysel, U.T., Bonhoeffer, T., and Hübener, M. (2013). Synaptic scaling and homeostatic plasticity in the mouse visual cortex in vivo. Neuron *80*, 327–334.

Kikuma, K., Li, X., Perry, S., Li, Q., Goel, P., Chen, C., Kim, D., Stavropoulos, N., and Dickman, D. (2019). Cul3 and insomniac are required for rapid ubiquitination of postsynaptic targets and retrograde homeostatic signaling. Nat. Commun. *10*.

Kiragasi, B., Wondolowski, J., Li, Y., and Dickman, D.K. (2017). A Presynaptic Glutamate Receptor Subunit Confers Robustness to Neurotransmission and Homeostatic Potentiation. Cell Rep. *19*, 2694–

2706.
Kittel, R.J., Wichmann, C., Rasse, T.M., Fouquet, W., Schmidt, M., Schmid, A., Wagh, D. a, Pawlu, C., Kellner, R.R., Willig, K.I., et al. (2006). Bruchpilot promotes active zone assembly, Ca2+ channel clustering, and vesicle release. Science *312*, 1051–1054.
Kulik, Y., Jones, R., Moughamian, A.J., Whippen, J., and Davis, G.W. (2019). Dual separable feedback systems govern firing rate homeostasis. Elife *8*, 1–27.
Li, X., Goel, P., Chen, C., Angajala, V., Chen, X., and Dickman, D.K. (2018). Synapse-specific and compartmentalized expression of presynaptic homeostatic potentiation. Elife *7*, e34338.
Liu, G., Choi, S., and Tsien, R.W. (1999). Variability of neurotransmitter concentration and nonsaturation of postsynaptic AMPA receptors at synapses in hippocampal cultures and slices. Neuron *22*, 395–409.
Maier, D., Hausser, A., Nagel, A.C., Link, G., Kugler, S.J., Wech, I., Pfizenmaier, K., and Preiss, A. (2006). Drosophila protein kinase D is broadly expressed and a fraction localizes to the Golgi compartment. Gene Expr. Patterns *6*, 849–856.
Maier, D., Nagel, A.C., Gloc, H., Hausser, A., Kugler, S.J., Wech, I., and Preiss, A. (2007). Protein Kinase D regulates several aspects of development in Drosophila melanogaster. BMC Dev. Biol. *7*, 1–13.
Muller, M., Liu, K.S.Y., Sigrist, S.J., and Davis, G.W. (2012). RIM Controls Homeostatic Plasticity through Modulation of the Readily-Releasable Vesicle Pool. J. Neurosci. *32*, 16574–16585.
Nagarkar-Jaiswal, S., Lee, P.T., Campbell, M.E., Chen, K., Anguiano-Zarate, S., Gutierrez, M.C., Busby, T., Lin, W.W., He, Y., Schulze, K.L., et al. (2015). A library of MiMICs allows tagging of genes and reversible, spatial and temporal knockdown of proteins in Drosophila. Elife *2015*, 1–28.
Olayioye, M.A., Barisic, S., and Hausser, A. (2013). Multi-level control of actin dynamics by protein kinase D. Cell. Signal. *25*, 1739–1747.
Ortega, J.M., Genç, Ö., and Davis, G.W. (2018). Molecular mechanisms that stabilize short term synaptic plasticity during presynaptic homeostatic plasticity. Elife *7*, 1–28.
Ouanounou, G., Baux, G., and Bal, T. (2016). A novel synaptic plasticity rule explains homeostasis of neuromuscular transmission. Elife *5*, 1–20.
Oueslati Morales, C., Ignácz, A., Bencsik, N., Rátkai, A.E., Lieb, W., Eisler, S., Schlett, K., and Hausser, A. (2020). PKD promotes activity-dependent AMPA receptor endocytosis in hippocampal neurons. BioRxiv.
Perry, S., Han, Y., Das, A., and Dickman, D. (2017). Homeostatic plasticity can be induced and expressed to restore synaptic strength at neuromuscular junctions undergoing ALS-related degeneration. Hum. Mol. Genet. *26*, 4153–4167.
Petersen, S.A., Fetter, R.D., Noordermeer, J.N., Goodman, C.S., and DiAntonio, A. (1997). Genetic analysis of glutamate receptors in Drosophila reveals a retrograde signal regulating presynaptic transmitter release. Neuron *19*, 1237–1248.
Piek, T. (1982). Δ-Philanthotoxin, a Semi-Irreversible Blocker of Ion-Channels. Comp. Biochem. Physiol. Part C, Comp. *72*, 311–315.
Schneggenburger, R., Meyer, A.C., and Neher, E. (1999). Released fraction and total size of a pool of immediately available transmitter quanta at a calyx synapse. Neuron *23*, 399–409.
Tatavarty, V., Torrado Pacheco, A., Groves Kuhnle, C., Lin, H., Koundinya, P., Miska, N.J., Hengen, K.B., Wagner, F.F., Van Hooser, S.D., and Turrigiano, G.G. (2020). Autism-Associated Shank3 Is Essential for Homeostatic Compensation in Rodent V1. Neuron *106*, 769–777.
Teichert, M., Liebmann, L., Hübner, C.A., and Bolz, J. (2017). Homeostatic plasticity and synaptic scaling in the adult mouse auditory cortex. Sci. Rep. *7*, 1–14.
Turrigiano, G.G. (2008). The Self-Tuning Neuron: Synaptic Scaling of Excitatory Synapses. Cell *135*, 422–435.
Turrigiano, G.G., Leslie, K.R., Desai, N.S., Rutherford, L.C., and Nelson, S.B. (1998). Activity-dependent scaling of quantal amplitude in neocortical neurons. Nature *391*, 892–896.
Twomey, E.C., Yelshanskaya, M. V, Vassilevski, A.A., and Sobolevsky, A.I. (2018). Mechanisms of

Channel Block in Calcium-Permeable AMPA Receptors. Neuron *99*, 956–968.
Valbuena, S., and Lerma, J. (2016). Non-canonical Signaling, the Hidden Life of Ligand-Gated Ion Channels. Neuron *92*, 316–329.
Wang, X., Pinter, M.J., and Rich, M.M. (2016). Reversible Recruitment of a Homeostatic Reserve Pool of Synaptic Vesicles Underlies Rapid Homeostatic Plasticity of Quantal Content. J. Neurosci. *36*, 828–836.
Wang, X., McIntosh, J.M., and Rich, M.M. (2018). Muscle Nicotinic Acetylcholine Receptors May Mediate Trans-Synaptic Signaling at the Mouse Neuromuscular Junction. J. Neurosci. *38*, 1725–1736.
Wentzel, C., Delvendahl, I., Sydlik, S., Georgiev, O., and Müller, M. (2018). Dysbindin links presynaptic proteasome function to homeostatic recruitment of low release probability vesicles. Nat. Commun. *9*, 267.
Weyhersmuller, A., Hallermann, S., Wagner, N., and Eilers, J. (2011). Rapid Active Zone Remodeling during Synaptic Plasticity. J. Neurosci. *31*, 6041–6052.
Yeates, C.J., Zwiefelhofer, D.J., and Frank, C.A. (2017). The Maintenance of Synaptic Homeostasis at the Drosophila Neuromuscular Junction Is Reversible and Sensitive to High Temperature. ENeuro *4*, e0220--17.2017.

Acknowledgement: We are grateful to members of the Müller lab for helpful discussions and critical comments on the manuscript. In particular, we would like to thank Igor Delvendahl and Olivier Urwyler for valuable input on earlier versions of this manuscript.
Funding: This research was funded by a Forschungskredit grant of the University of Zurich and an International Postdoc grant (2018-06813) by Swedish Research Council to AGN, as well as a Swiss National Science Foundation Assistant Professor grant (PP00P3–15), and an European Research Council Starting grant (SynDegrade-679881) to MM.
Author Contributions: MM and AGN conceptualized and designed experiments. AGN and PM conducted research, analyzed data. AGN, PM and MM interpreted data. MM and AGN wrote the manuscript.
Competing Interests: The authors declare no competing interests.
Data Availability: All data needed to evaluate the conclusions in the paper are present in the paper and the Supplementary Materials

Supplementary Material

A *DKaiR1D*[2]

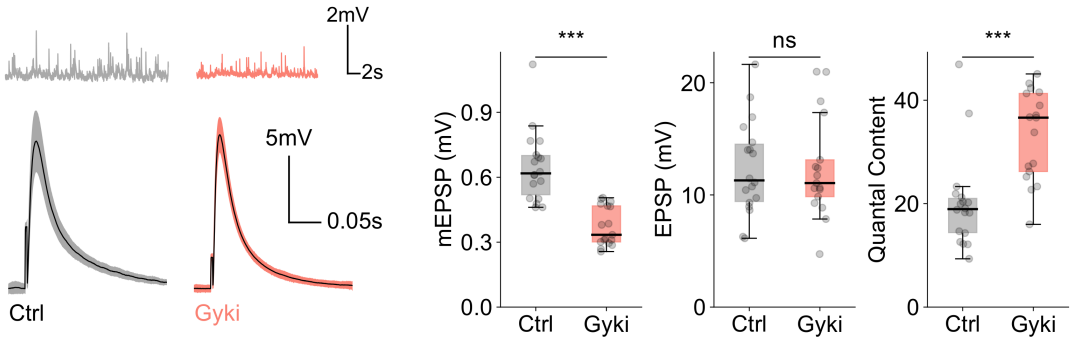

Fig. S1. *Gyki induces PHP at NMJs with mutant kainate receptor subunit R1D. (**A**) Representative traces (mEPSPs and EPSPs), mEPSP amplitudes, EPSP amplitudes, and quantal content of saline (Ctrl) or Gyki-treated kainate receptor subunit R1D, DKaiR1D, mutant NMJs. Gyki treatment results in PHP, as indicated by an increased quantal content. n = 18 (Ctrl) vs 17 (Gyki). $[Ca^{2+}]_e$ = 0.3 mM. Pairwise comparisons were done with a two-sided Mann Whitney U test. Each data point indicates the median value for a given cell. ns : p >= 0.05; * : p < 0.05; ** : p < 0.01; *** : p < 0.001.*

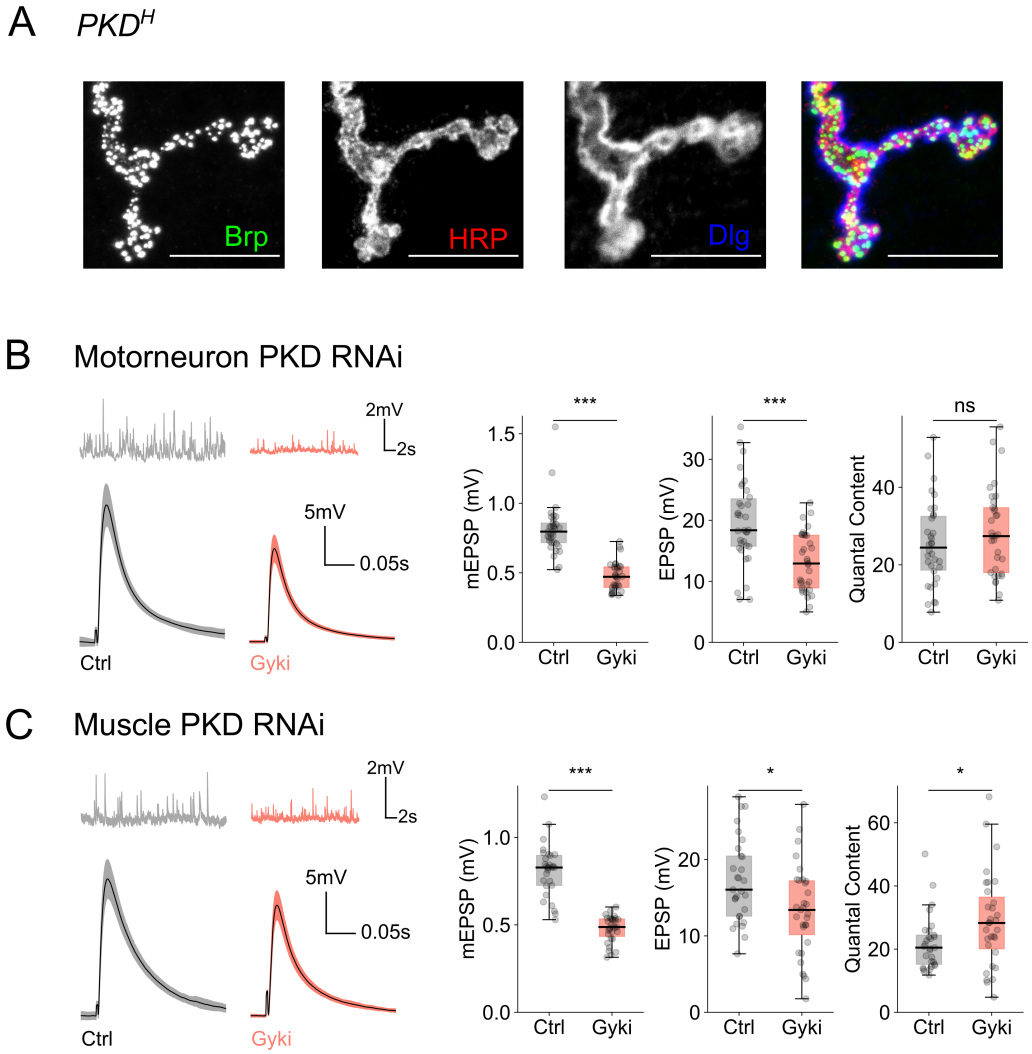

Fig. S2. *Involvement of presynaptic PKD in Gyki-induced PHP.* (***A***) *Immunostaining of a PKD^H mutant NMJ (max. intensity projection). NMJs were stained for the active-zone marker Bruchpilot (Brp), neuronal membrane (HRP), and the postsynaptic reticulum (Dlg). Scale bar = 10 µm. The staining shows no gross morphological defects in PKD^H mutant NMJ.* (***B***) *Representative traces (mEPSPs and EPSPs), mEPSP amplitudes, EPSP amplitudes and quantal content of saline (Ctrl) or Gyki-treated NMJs after presynaptic motorneuron PKD RNAi expression. There was no increase in quantal content after Gyki treatment, indicating impaired in Gyki-induced PHP. n = 34 (Ctrl) vs 33 (Gyki). $[Ca^{2+}]_e$ = 0.3 mM.* (***C***) *Representative traces (mEPSPs and EPSPs), mEPSP amplitudes, EPSP amplitudes and quantal content of saline (Ctrl) or Gyki-treated NMJs after postsynaptic muscle PKD RNAi expression. Quantal content increased in the presence of Gyki, indicating PHP induction in response to Gyki. n = 29 (Ctrl) vs 31 (Gyki). $[Ca^{2+}]_e$ = 0.3 mM. Pairwise comparisons were done with a two-sided Mann Whitney U test. Each data point indicates the median value for a given cell. ns : p >= 0.05; * : p < 0.05; ** : p < 0.01; *** : p < 0.001.*